Predictive screening of phase stability in high-entropy ceramics

Muhammad Waqas Qureshi[1, *], Shuguang Wei[1], Longfei Liu[1], Sudipta Paul[1], Jun Young Kim[1], Chuan Zhang[2], Xudong Wang[1], John H. Perepezko[1], Dane Morgan[1], Izabela Szlufarska[1, *]

[1] Department of Materials Science and Engineering, University of Wisconsin-Madison, WI 53706, United States

[2] CompuTherm LLC, Madison, WI 53562, United States

*Corresponding authors: *mwqureshi2@wisc.edu (MWQ), *szlufarska@wisc.edu (I. Szlufarska)

I. Determination of kinetic temperature (T_k) for free energy

In synthesis temperatures for HEBs and HECs range from 1800 ℃ to 2200 ℃ and samples are furnace-cooled. It is unknow at what temperature during cooling, the kinetics freeze and the material solidifies into a solid-state phase encountered at that temperature. This temperature is referred to as the kinetic temperature (T_k). T_k is not known in general, but for sintering and annealing of multicomponent ceramics, it is typically taken as approximately half of the average melting point of the corresponding binary carbides/borides[1,2]. We used a similar approach to estimate T_k for the purpose of our free-energy model. Here, we define T_k as:

$$T_k = \frac{1}{n}\sum_{i=1}^{n} T^{binary}_{m,\,i}$$

where $T^{binary}_{m,\,i}$ is the melting temperature of the i^{th} binary carbide or boride, and n is the total number of binaries considered. The values of T_k of each composition are rescaled to constrain them within the range of 1200 ℃ to 1600 ℃, using the following expression

$$T^{i}_{k} = 1200 + \frac{\left(T_k - T^{min}_{k}\right)}{\left(T^{max}_{k} - T^{min}_{k}\right)} \times 400$$

where T^{i}_{k} is the final kinetic temperature for a given composition of HEBs and HECs used in the free-energy model. T^{min}_{k} and T^{max}_{k} are the minimum and maximum T_k among the HEBs and HECs compositions considered in our study.

In the main text of the manuscript, we showed predictions of our DFT-based free energy model at T_k estimated, as explained above. Here, for testing purposes, we calculated the free energy for HECs at three fixed temperatures ranging from 1200 ℃ to 2000 ℃ with a step size of 100 ℃. As we increase the temperature, the number of outliers near $\Delta G = 0$ increases slightly, which results in a slight decline in the F1 score from 0.97 to 0.89 for HEBs and 0.95 to 0.92 for HECs, respectively (Fig. S1). Since T_k is generally unknown, we have estimated it using a general principle that diffusion kinetics in a multi-component carbide/boride is strongly correlated with the melting temperatures of corresponding binary carbides/borides, as done previously in literature and explained above.

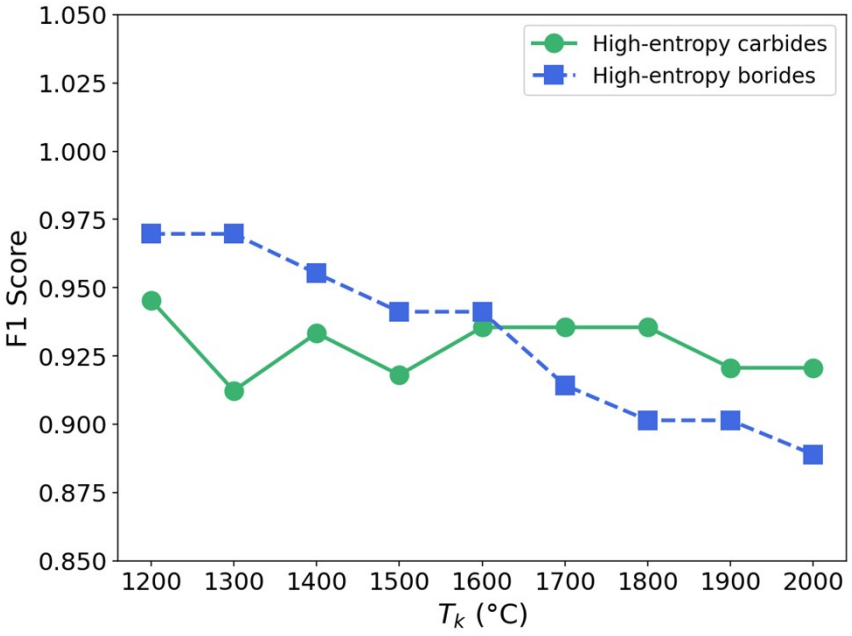

Figure S1. Accuracy of the free-energy model at fixed temperaures. *F1 score for predictions of HECs at fixed temperatures (T_k) from 1200 ℃ to 2000 ℃ with the step size of 100 ℃.*

II. Bond separation energy of MB_2 phases

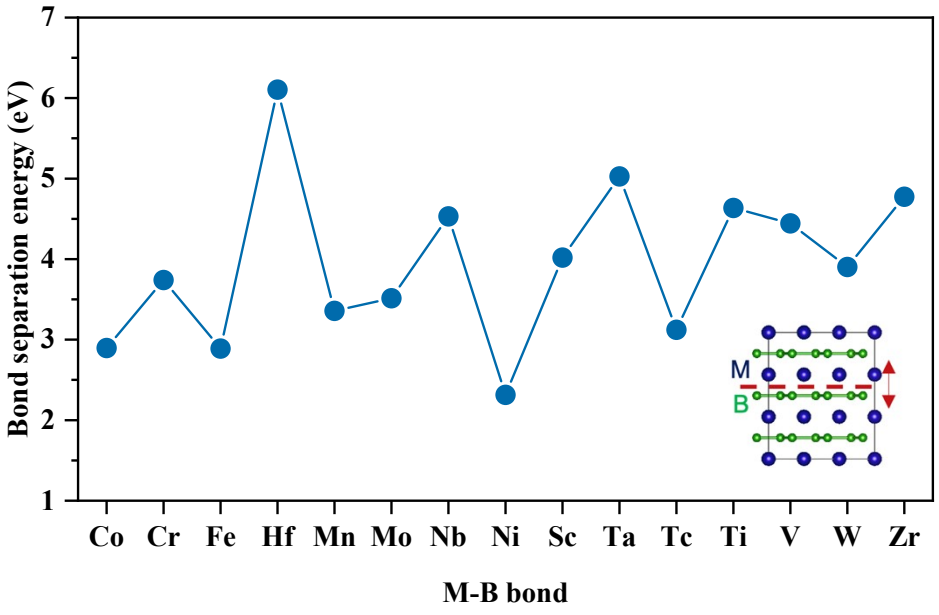

Figure S2. DFT calculated bond separation energy for M-B bond in AlB_2 prototype strucure*.The bond separation energy is calculated by following the methodology in Ref[3], in which the energy difference of a perfect unit cell and unit cell with 2 nm vacuum between the layers is divided by the number of surfcae atoms.*

III. Experimental disagreement of W-based HEBs

HEBs containing W have atypical behavior and contradictory experimental observations have been reported in literature as to whether they can form single-phase[4–8]. For example, a W-rich secondary phase has been observed in $(TiZrHfMoW)B_2$ after synthesis either from conventional spark plasma sintering of individual binary borides[9] or from borocarbothermal reduction of metal oxides[10]. CALPHAD phase diagrams classify this composition as multi-phase because it contains two types of phases (MB_2_hP3 and W_2B_5) at 1:2 stoichiometry of diboride (see composition $(HfMoTiWZr)B_2$ in Fig S8). In contrast, $(CrMoTaTiW)B_2$, $(HfNbTaWZr)B_2$, and $(HfMoTaWZr)B_2$ were found to be both single-phase[5] and multi-phase[5], depending on the synthesis route. However, one of the authors of Ref.[5] later found the material initially identified as "single-phase" material had W-rich precipitation at the grain boundaries [11]. These results highlight some of the challenges associated with experimental synthesis of high-entropy ceramics, especially W containing HEBs and the need for a detailed microstructural analysis of synthesized samples.

IV. Energy dispersive X-ray spectroscopy (EDS) measurement of elemental distribution

Electron dispersion spectroscopy (EDS) point scan was also collected in (TiZrHfMoW)C to check the homogeneity of elemental distribution. We collected point scans at 4 different positions (Fig. S3). The percentages of each metal in cation sublattice are listed in Table S4. We found that the difference of composition between 4 points is within the equipment error, suggesting sufficient homogeneity of elements in annealed (TiZrHfMoW)C.

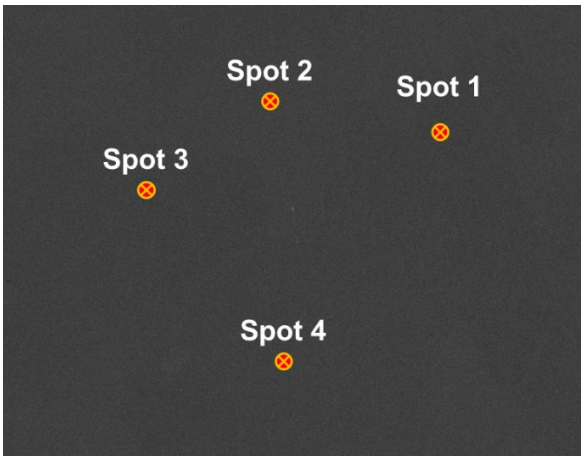

Figure S3. SEM-based electron dispersion spectroscopy (EDS). *SEM image showing positions of EDS point scan collection in (TiZrHfMoW)C HEC sample.*

V. Comparison between *ab-initio* based free energy model and CALPHAD calculations

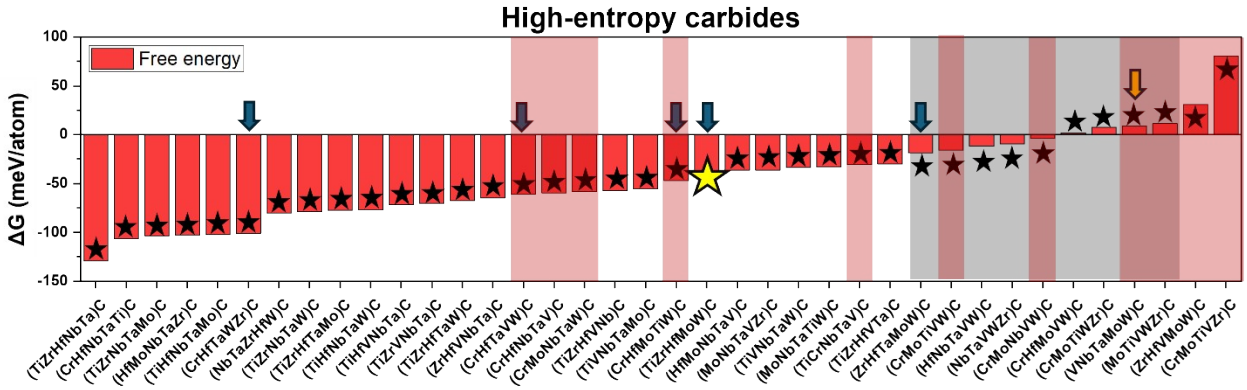

Figure S4. Predictions of phase stability in HECs. *A comparison of free energies predicted using ab initio based free energy model with CALPHAD (pink vertical bars) for the same data as shown in Figure 3(a) of the main text. The negative and positive values of ΔG indicate single- and multi-phase stability, respectively. Black stars mark experimental data available in literature. Arrows indicate compositions where published experimental data seemingly disagree with predictions of our model, all W-based HECs. Yellow star marks HEC composition ((TiZrHfMoW)C) synthesized by us that confirms single-phase stability predicted by our model. Grey regions corresponds to a 20 meV buffer that represents uncertainty in predictions of the model due to approximations in calculations of free energy.*

VI. Density functional theory (DFT)-based descriptors

There have been significant efforts in predicting the phase stability of high-entropy ceramics through different DFT-based descriptors. These descriptors include entropy forming ability (EFA)[12], lattice distortion, disordered enthalpy-entropy descriptors (DEED)[4], lattice distortion, and a number of additional descriptors i.e., valance electron concentration (VEC)[13], Zunger pseudopotential radii (P_{rad})[14], and Pauling electronegativity difference ($\Delta\chi_{Pauling}$)[14]. Here, we assess the suitability of some of the previously proposed descriptors for HEBs considered in our study. Figure S6a shows the reciprocals of EFAs where diamond symbols represent W-based HEBs that had mixed experimental reports as discussed in section III and shown in Table S2. Data points corresponding to single-phase materials are marked as black squares, whereas multi-phase materials are marked as red circles, and this determination was based on our CALPHAD calculations. The CAPLHAD data shown in the plot agrees with our *ab-initio* free energy model. Data is clustered into two groups. Single-phase HEBs generally have a lower EFA^{-1}, and multi-phase HEBs have a higher EFA^{-1}. There exists a misclassification regime, indicated by a shaded grey region, where several HEBs of single- and multi-phase are mixed. Our analysis shows that EFA^{-1} is a good predictor of phase stability for extreme values, far from the transition region. Once again, W-based compositions appear to be the exception.

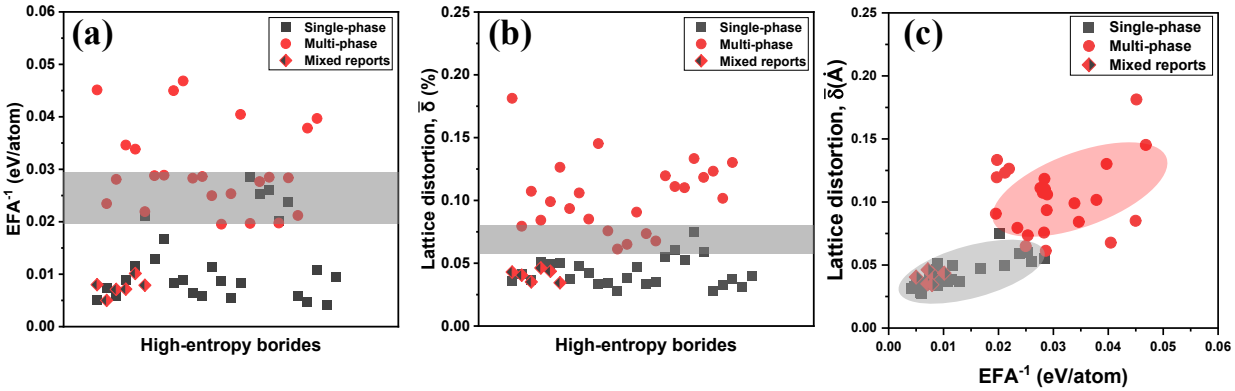

Figure S5. DFT-based descriptors for phase stability of HEBs. *(a) Reciprocal of EFA (b) Lattice distortion, and (c) Relationship between lattice distortion and EFA^{-1}. Black squares and red circles represent single-phase and multi-phase compositions, respectively. Dual colored diamonds correspond to mixed experimental reports. Grey shaded area in (a) and (b) represent the misclassification regimes.*

Figure S6b presents the average lattice distortion ($\bar{\delta}$) for all HEB compositions considered in this study. We quantify the lattice distortion of HEBs by relaxing the supercell in two stages. First, only lattice parameters are relaxed and subsequently, both lattice parameters and atom positions are relaxed (see section VII for more details). We find that the distribution of lattice distortions for all HEBs can be separated into two regions: single-phase materials tend to have a small lattice distortion, and multi-phase materials tend to have a large lattice distortion. Similarly to EFA, there is still a misclassification region, highlighted in grey. For VEC, P_{rad}, and $\Delta\chi_{Pauling}$ the misclassification regime is significantly wider than for EFA^{-1} and lattice distortion (see Fig. S7), suggesting that these three descriptors are not as effective in predicting the phase stability. It has been previously suggested for HECs that EFA^{-1} and lattice distortion are linearly correlated[12]. We do not find this correlation to be compelling in the case of HEBs (see Fig. S6c).

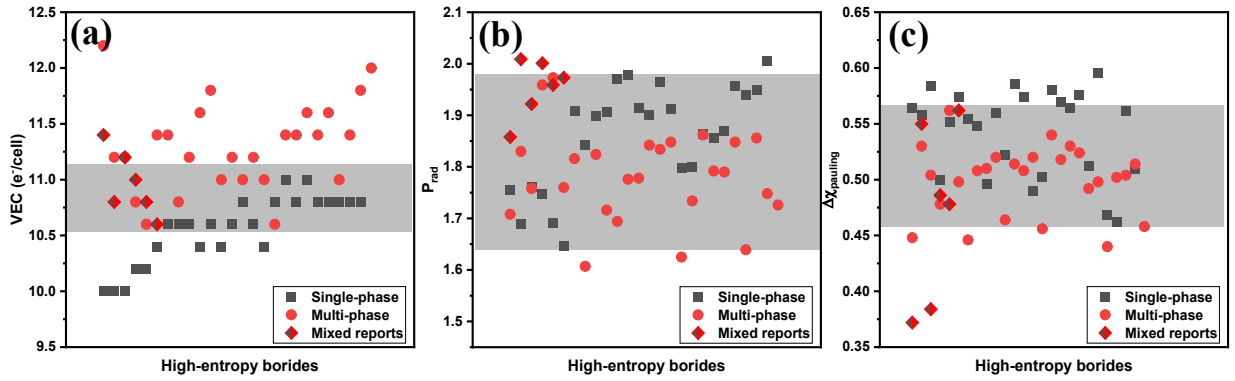

Figure S6. Additional descriptors for phase stability of HEBs. *(a) Valance electron concentration, VEC (b) Zunger pseudopotential radii, P_{rad} and (c) Pauling electronegativity difference $\Delta\chi_{Pauling}$. Black squares and red circles represent the single phase and multi-phase*

compositions, respectively. Dual colored diamonds are experimental mixed reports data. Grey shaded area represents a misclassification regime.

In Fig. S7a we show DEED descriptor, which has been proposed for high-entropy borides and carbonitrides[4]. All the values of DEED for HEBs are taken from the Ref.[4] and we included data for most of the experimentally synthesized HEB compositions. DEED effectively orders the experimentally observed single- (high DEED value) and multi-phase (low DEED value) HEBs. This trend becomes obvious when the data from the mixed report are excluded (see Fig. S7b). Figure S7c shows a phase comparison between DEED and our CALPHAD predictions for all available experiments, as well as some of our compositions for which DEED values are reported in Ref[4]. It is worth mentioning that our CALPHAD data shown in the plots are consistent with *ab-initio* based free energy model. Compositions circled with red dashed line have high DEED values showing consistency with phase diagram predictions. However, compositions circled with black dashed line seemingly disagree with phase diagram. These compositions are predicted to be single-phase by both CALPHAD and our *ab initio* based free energy model but have low DEED values (suggesting multi-phase HEB). These compositions are HEB-MnMo, HEB-MnTa, HEB-MnNb, and HEB-CrV.

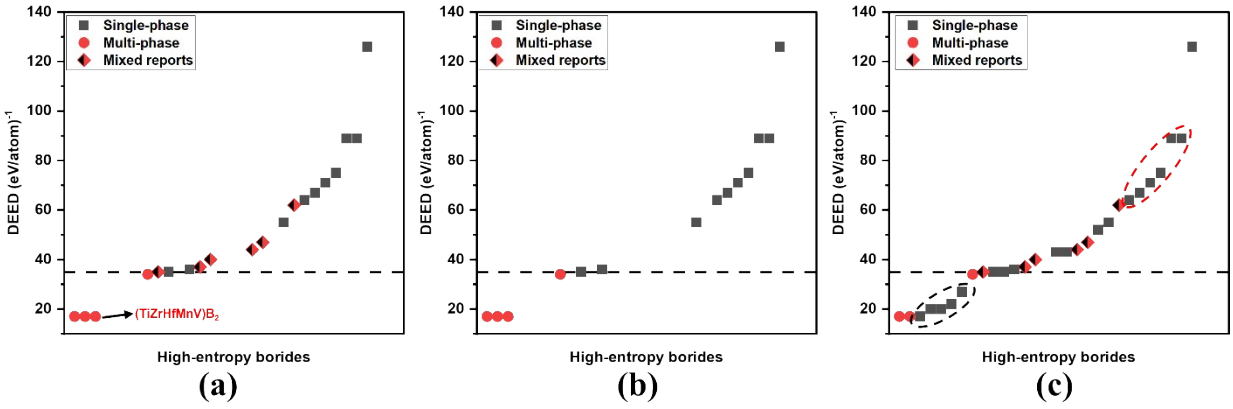

Figure S7. DEED descriptor for phase stability of HEBs. *(a) DEED for all of the available experimental data. (b) The same data as in (a) after excluding data corresponding to mixed experimental reports. (c) Comparison between DEED and CALPHAD predictions . The horizontal dashed line is the threshold value for DEED to predict single-phase compositions set in Ref[4].*

VII. Calculation of DFT-based descriptors

In order to calculate EFA, AFLOW-POCC algorithm[15] implemented within the framework of AFLOW computational materials design[16–18], is used to generate the sampled configurations. For each HEB and HEC composition, AFLOW-POCC generates a total of 82 and 49 unique configurations using Hermite normal form matrices. Each configuration contains the minimum size of cell necessary to produce the required stoichiometry: one atom of each of the metal and 10 boron atoms for HEB and one atom of each of the metal and 5 carbon atoms for HEC. To obtain energy distribution, all the unique configurations are fully relaxed.

Lattice distortions are calculated in two stage relaxation process. In the first stage, only lattice parameters of special quasirandom structure (SQS) structure are relaxed until the maximum stress tensor component was smaller than 10^{-3} eV/Å^3. The structure is relaxed with internal forces while maintaining approximately zero external stress and lattice distortion. In the second stage, both lattice parameters and atomic positions are relaxed to achieve zero external stress, internal forces, and lattice distortion. From the two-stage relaxation, the displacement of atoms from the ideal lattice site can be calculated as:

$$\Delta r = \begin{bmatrix} \Delta x \\ \Delta y \\ \Delta z \end{bmatrix} = (u - u_0).a + (v - v_0).b + (w - w_0).c \quad \text{(S1)}$$

where *u, v* and *w,* are the final lattice sites (second stage relaxation) and u_0, v_0 and w_0, are the ideal lattice sites (first stage relaxation). *a*, *b*, and *c* are the lattice parameters of the fully relaxed SQS structures. The total lattice distortion is defined as

$$\delta = \|\Delta r\|_2 = \sqrt{\Delta x^2 + \Delta y^2 + \Delta z^2} \quad \text{(S2)}$$

VIII. CALPHAD phase diagrams of high entropy borides (HEBs) and carbides (HECs)

Equilibrium phase diagrams of high-entropy ceramics considered here were calculated using the recently updated PanRHEA2023b thermodynamic database and Pandat software (version 2023)[19] developed by CompuTherm, LLC. The PanRHEA2023b database contains 22 elements with 509 phases and has complete thermodynamic descriptors for all the binary systems (especially metal diboride and carbides) which build up the quinary HEB systems explored in this work.

Figures S8-S11 illustrate CALPHAD predictions of phase stability for high entropy borides (HEBs) and carbides (HECs). We are showing phase regions ranging from 65-70 at% of boron and 35-55 at% of carbon for HEBs and HECs, respectively. The compositions are predicted to be single- or multi-phase based on the number and types of phases at stoichiometry of diboride (1:2) and carbide (1:1) in the entire temperature range. Single-phase HEBs and HECs have the phase region consisting of only "MB_2_hP3" and "FCC" phase, respectively, whereas multi-phase compositions show the phase region with a mixture of complex phases.

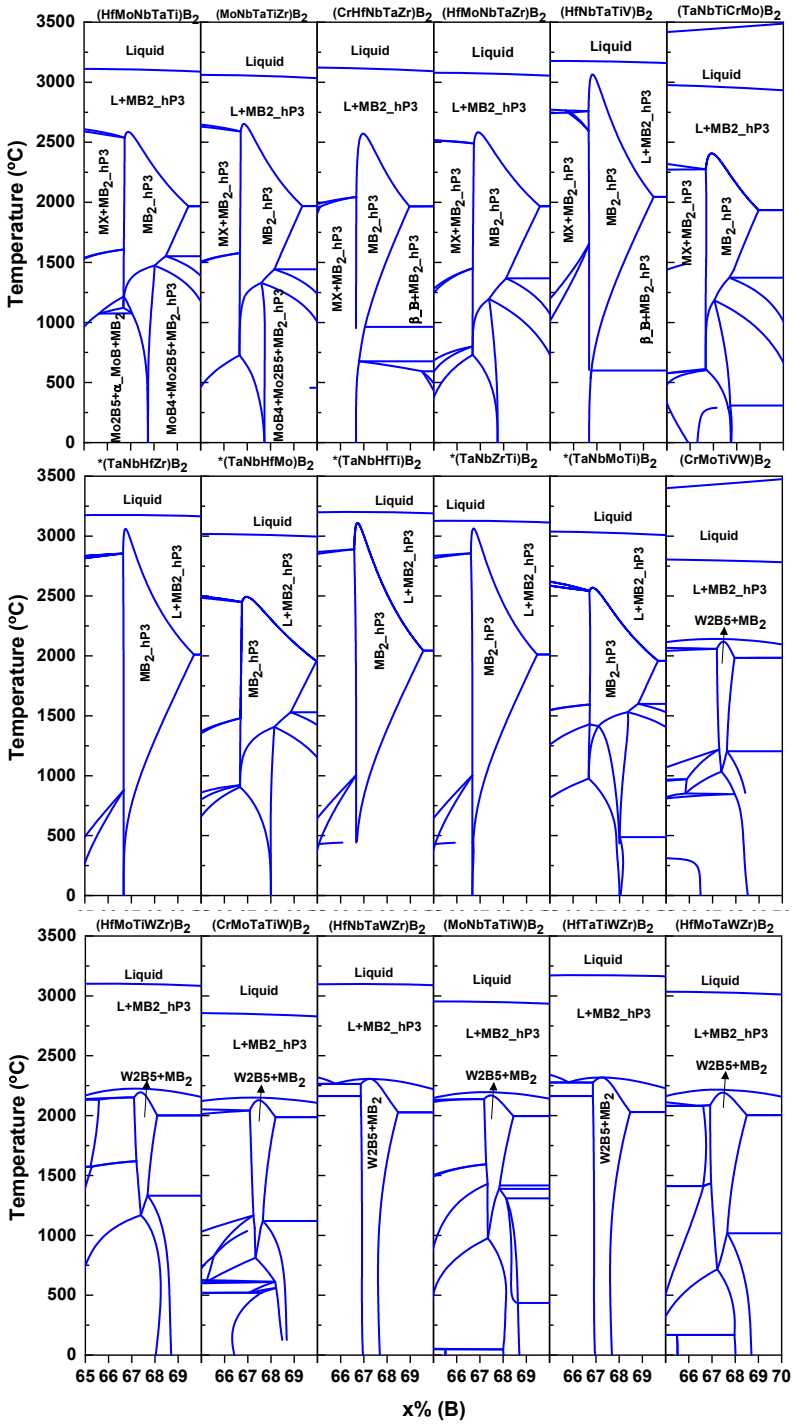

Figure S8. CALPHAD phase diagrams for experimentally synthesized HEBs*. CALPHAD predictions of phase stability for HEB compositions which have been synthesized experimentally[4,6,9,10,20–22] and are being considered in our ab initio based free energy model. Text on top and inside of the phase diagrams represents the HEB composition and type of phases in each region, respectively). The compositions with * in their names are the quaternary compositions with 4-components. Letter "L" stands for liquid phase.*

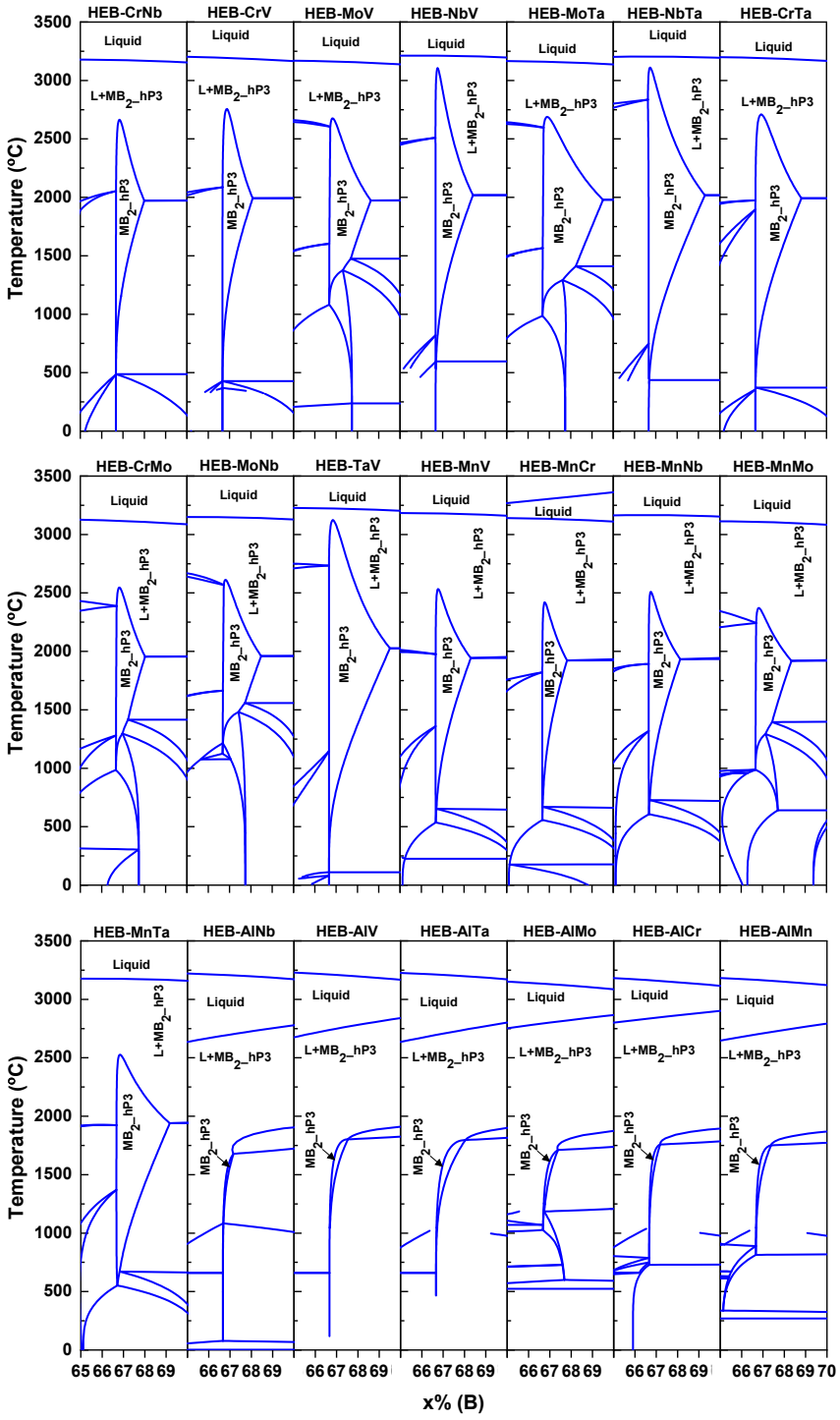

Figure S9. CALPHAD phase diagrams for single-phase HEBs*. Phase diagrams HEBs which are predicted to be single-phase from CALPHAD calculations. In these phase diagrams a region with only one phase "MB_2_hp3" is observed at around 66.67 at% of B at any temperature. Text on top and inside of the phase diagrams represents the HEB composition and type of phases in each region, respectively. Letter "L" stands for liquid phase.*

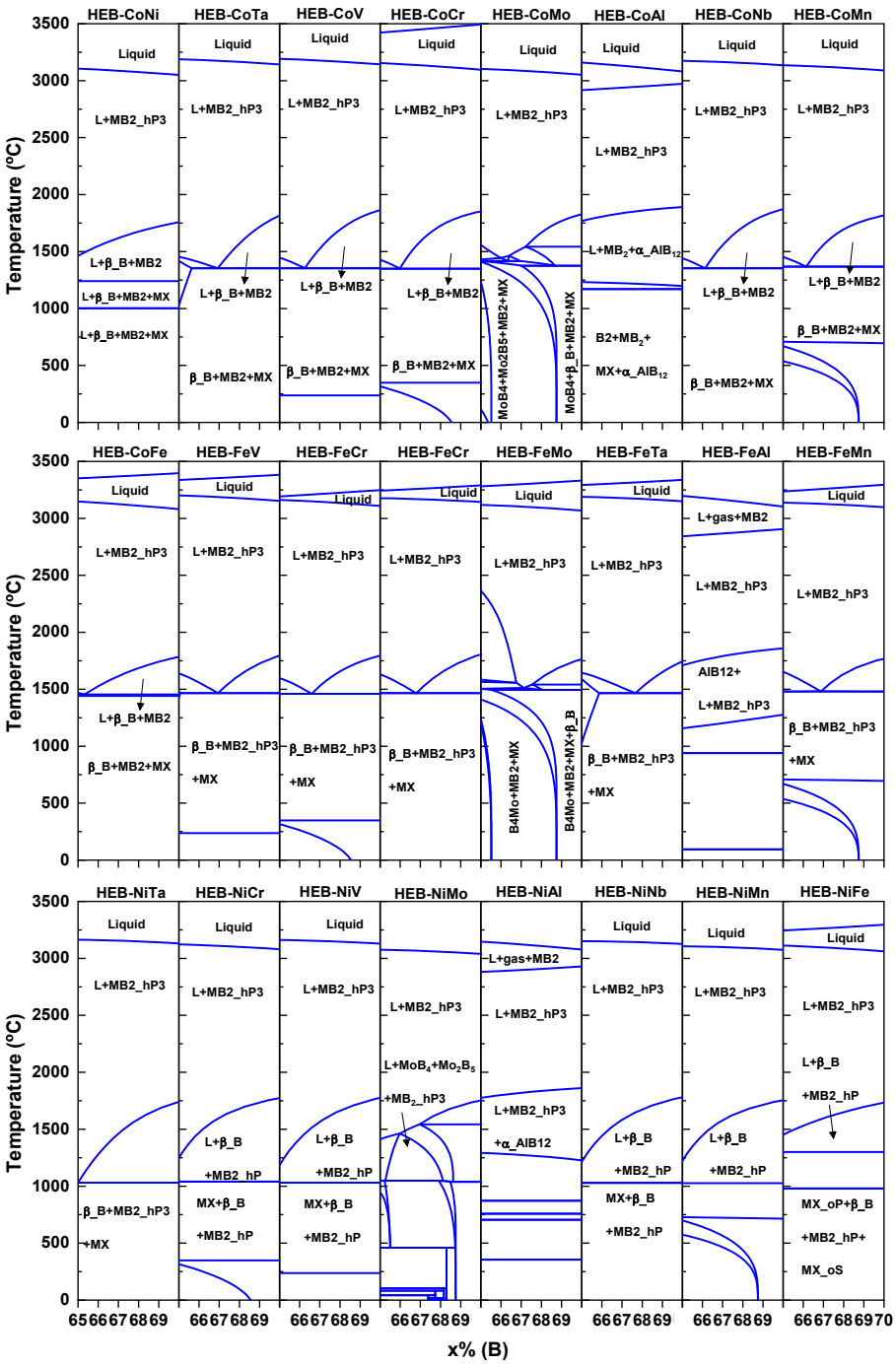

Figure S10. CALPHAD phase diagrams for multi-phase HEBs*. Phase diagrams for HEBs that are predicted to be multi-phase from CALPHAD calculations. In these phase diagrams more than one phase coexists in the phase region at around 66.67 at% of B at any temperature. Text on top and inside of the phase diagrams represents the HEB composition and type of phases in each region, respectively. Letter "L" stands for liquid phase.*

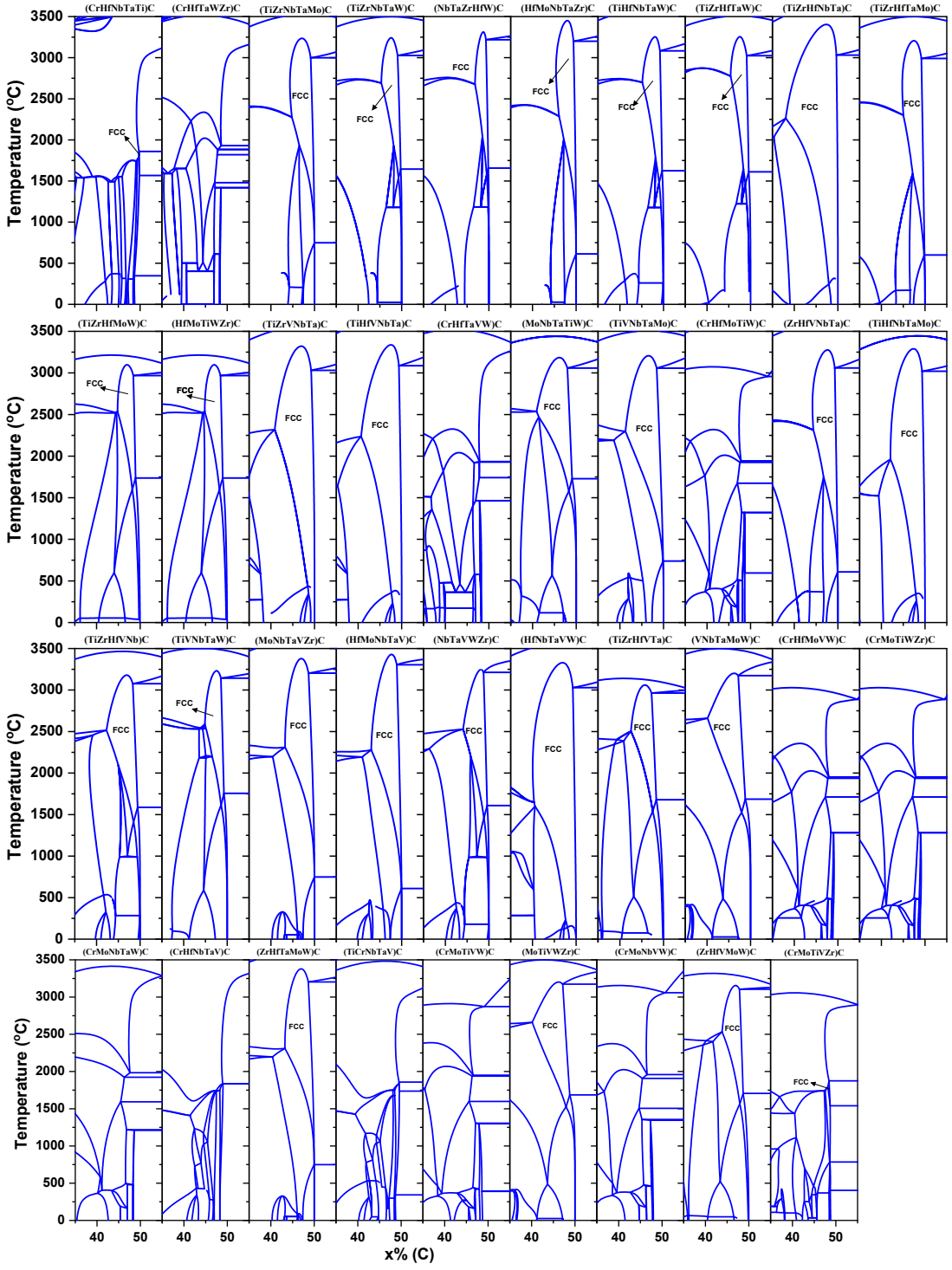

Figure S11. CALPHAD phase diagrams for HECs*. Phase diagrams predictions from CALPHAD calculations. Single phase region is denoted by "FCC". Text on top and inside of the phase diagrams represents the HEC composition.*

Table S1. Estimation of temperature for ab-initio based free energy model*. The melting point of binary carbides and diborides, average melting point of high-entropy materials and the values of T_k for all the materials estimated from linear function. All the values are in ℃.*

	Carbides				***Borides***			
Elements	Binary	Composition	Average	T_k	Binary	Composition	Average	T_k
Ti	3160	(TiZrHfNbTa)C	3590.4	1600	3230	HEB-NbTa	3193.6	1600
Zr	3532	(CrHfNbTaTi)C	3284	1466.75	3246	HEB-NbMo	3053	1503.46
Hf	3900	(TiZrNbTaMo)C	3386.6	1511.37	3377	HfNbTaTiV	3094.4	1531.89
V	2810	(HfMoNbTaZr)C	3461	1543.73	2750	HEB-CrTa	3022.4	1482.45
Nb	3480	(TiHfNbTaMo)C	3386.6	1511.37	3028	HEB-NbCr	3010.6	1474.35
Ta	3880	(CrHfTaWZr)C	3236.4	1446.05	3087	HfMoNbTaZr	3024.4	1483.83
Cr	2000	(NbTaZrHfW)C	3532.4	1574.78	2172	HEB-MnTa	2955.4	1436.45
Mo	2513	(TiZrNbTaW)C	3384.4	1510.42	2384	HEB-MnNb	2943.6	1428.35
W	2870	(TiZrHfTaMo)C	3397	1515.89		ErHfTaTiZr	2938.3	1424.71
Mn		(TiHfNbTaW)C	3458	1542.42	1837	MoNbTaTiZr	2995	1463.64
Al		(TiHfVNbTa)C	3446	1537.2	1030	HEB-CrMo	2881.8	1385.92
		(TiZrVNbTa)C	3372.4	1505.2		HEB-NbV	3126.2	1553.72
		(TiZrHfTaW)C	3468.4	1546.94		HfMoNbTaTi	3021.2	1481.63
		(ZrHfVNbTa)C	3520.4	1569.56		TaNbHfZr	3184.5	1593.75
		(CrHfTaVW)C	3092	1383.26		TaNbHfTi	3180.5	1591.00
		(CrHfNbTaV)C	3214	1436.31		HEB-FeTa	2938.3	1424.71
		(CrMoNbTaW)C	2948.6	1320.9		TaNbZrTi	3147.75	1568.52
		(TiZrHfVNb)C	3376.4	1506.94		HEB-TaMo	3064.8	1511.56
		(TiVNbTaMo)C	3168.6	1416.57		HEB-AlNb	2782.2	1317.54
		(CrHfMoTiW)C	2888.6	1294.8		TaNbTiMo	2932.25	1420.56
		(TiZrHfMoW)C	3195	1428.05		HEB-VTa	3138	1561.82
		(HfMoTiWZr)C	3195	1428.05		TaNbHfMo	2969	1445.79
		(HfMoNbTaV)C	3316.6	1480.93		HEB-MnMo	2814.8	1339.92
		(MoNbTaVZr)C	3243	1448.92		HEB-VCr	2955	1436.18
		(TiVNbTaW)C	3240	1447.62		TaNbTiCrMo	2780.2	1316.16
		(MoNbTaTiW)C	3180.6	1421.79		HEB-AlTa	2794	1325.64
		(TiCrNbTaV)C	3066	1371.95		HEB-AlMo	2653.4	1229.11
		(TiZrHfVTa)C	3456.4	1541.73		HEB-VMo	2997.4	1465.29
		(ZrHfTaMoW)C	3339	1490.67		HEB-MnV	2888	1390.18
		(CrMoTiVW)C	2670.6	1200		HEB-AlCr	2611	1200
		(HfNbTaVW)C	3388	1511.98		HEB-FeMo	2938.3	1424.71
		(NbTaVWZr)C	3314.4	1479.97		HEB-AlV	2726.6	1279.36
		(CrMoNbVW)C	2734.6	1227.83		HEB-MnAl	2938.3	1424.71
		(CrHfMoVW)C	2818.6	1264.36		HEB-MnCr	2772.4	1310.81
		(CrMoTiWZr)C	2815	1262.8		HEB-FeV	2938.3	1424.71
		(VNbTaMoW)C	3110.6	1391.35		HEB-FeAl	2938.3	1424.71
		(MoTiVWZr)C	2977	1333.25		HEB-NbCo	2938.3	1424.71
		(ZrHfVMoW)C	3125	1397.61		HEB-FeCr	2938.3	1424.71

		(CrMoTiVZr)C	2803	1257.58		HEB-NbNi	2938.3	1424.71
						HEB-NiMo	2938.3	1424.71
						HEB-NiTa	2938.3	1424.71
						HEB-CoMo	2938.3	1424.71
						HEB-FeMn	2938.3	1424.71
						HEB-CoCr	2938.3	1424.71
						HEB-CrNi	2938.3	1424.71
						HEB-FeNb	2938.3	1424.71
						HEB-MnCo	2938.3	1424.71
						HEB-CoTa	2938.3	1424.71
						HEB-MnNi	2938.3	1424.71
						HEB-CoV	2938.3	1424.71
						HEB-NiV	2938.3	1424.71
						HEB-FeNi	2938.3	1424.71
						HEB-AlCo	2938.3	1424.71
						HEB-AlNi	2938.3	1424.71
						HEB-FeCo	2938.3	1424.71
						HEB-CoNi	2938.3	1424.71

Table S2. Summary of experimental observations, predictions of ab initio based free energy, and CALPHAD calculations for HEBs*. Text in bold highlights special cases where there appears to be disagreement either between different experiments or between experiments and our CALPHAD predictions.*

Composition	**Experiment**	**CALPHAD**	***Ab inito* based free energy model**	**Remarks**
	Single Phase	**Single Phase**	**Single phase**	
HEB-NbTa	Yes[9]	Yes	Yes	
HEB-MoTa	Yes[9]	Yes	Yes	
HEB-NbMo	Yes[9]	Yes	Yes	
HEB-CrTa	Yes[9]	Yes	Yes	
HEB-TaV	Yes[23]	Yes	Yes	
(HfMoNbTaTi)B_2	Yes[9]	Yes	Yes	
(MoNbTaTiZr)B_2	Yes[9]	Yes	Yes	
(HfMoNbTaZr)B_2	Yes[4,22]	Yes	Yes	
(HfNbTaTiV)B_2	Yes[4]	Yes	Yes	
(CrHfNbTiZr)B_2	Yes[4]	Yes	Yes	
(TaNbTiCrMo)B_2	Yes[24]	Yes	Yes	
(TaNbHfZr)B_2	Yes[24]	Yes	Yes	
(TaNbHfMo)B_2	Yes[24]	Yes	Yes	
(TaNbHfTi)B_2	Yes[24]	Yes	Yes	

$(TaNbZrTi)B_2$	Yes[24]	Yes	Yes	
$(TaNbTiMo)B_2$	Yes[24]	Yes	Yes	
$(HfMnTiVZr)B_2$	**No**[4]	**Yes**	Yes	
$(TiZrHfTaEr)B_2$	Yes[21]	--		Er segregation observed at grain boundaries in experiments.
$(CrMoTiVW)B_2$	**Yes**[4]	**No**		Small amount of residual carbon+B_4C was found in experiments.
$(HfMoTiWZr)B_2$	No[9,10,20]	No		Ti–Mo–W rich secondary phase observed in experiments.
$(CrMoTaTiW)B_2$	**Yes/No**[5]	**No**		Multi-phase via SPS and single-phase via boron-metal reactive sintering.
$(HfNbTaWZr)B_2$	**Yes/No**[5]	**No**		
$(HfMoTaWZr)B_2$	**Yes/No**[5]	**No**		
$(MoNbTiTaW)B_2$	**Yes**[6]	**No**		Detailed microstructure analysis was not conducted
$(HfTaTiWZr)B_2$	No[11,23]	No		Grain boundary segregation and precipitation of W observed in experiments.

Table S3. List of HEBs predicted to be single-phase. *The list of the HEBs that are predicted to be stable in single phase solid solutions from our ab initio free energy model. The compositions which have not been reported elsewhere are highlighted in bold text.*

Compositions		
HEB-MnNb	**HEB-AlTa**	HEB-MnNb
HEB-MnTa	**HEB-AlMo**	HEB-CrNb
HEB-CrMo	**HEB-AlCr**	HEB-CrTa
HEB-AlNb	**HEB-MoV**	HEB-NbTa
HEB-NbV	**HEB-AlV**	HEB-MoTa
HEB-MnMo	**HEB-AlMn**	HEB-TaV
HEB-CrV	**HEB-CrMn**	HEB-MnV

Table S4. SEM-based EDS point scan. *The percentages of each metal in cation sublattice for (TiZrHfMoW)C to confirm the homogeneity of elemental distribution. Figure. S5 shows the locations where these point EDS spots are taken.*

Point EDS spot	**Composition (%)**				
	Ti	**Zr**	**Hf**	**Mo**	**W**
1	22.28	21.38	20.85	19.28	16.21
2	22.54	21.41	22.84	17.22	15.99
3	22.77	21.37	19.83	19.74	16.3
4	22.63	21.27	21.4	18.51	16.19

References

1 A. C. Feltrin, D. Hedman and F. Akhtar, *Appl Phys Lett*, 2021, **119**, 161905.

2 L. Ran, S. Guan, W. Liang, J. Pu, P. He, H. Long, P. Yang and F. Peng, *Journal of the American Ceramic Society*, 2025, **108**, 20368–20374.

3 J. Y. Kim, H. Zhang, J. Xi and I. Szlufarska, *Chemistry of Materials*, 2022, **34**, 7807–7816.

4 S. Divilov, H. Eckert, D. Hicks, C. Oses, C. Toher, R. Friedrich, M. Esters, M. J. Mehl, A. C. Zettel, Y. Lederer, E. Zurek, J.-P. Maria, D. W. Brenner, X. Campilongo, S. Filipović, W. G. Fahrenholtz, C. J. Ryan, C. M. DeSalle, R. J. Crealese, D. E. Wolfe, A. Calzolari and S. Curtarolo, *Nature 2024 625:7993*, 2024, **625**, 66–73.

5 M. Qin, J. Gild, H. Wang, T. Harrington, K. S. Vecchio and J. Luo, *J Eur Ceram Soc*, 2020, **40**, 4348–4353.

6 D. Liu, H. Liu, S. Ning and Y. Chu, *Journal of Advanced Ceramics*, 2020, **9**, 339–348.

7 S. Dong, Q. Li, H. Hu, X. Zhang, Y. Li, K. Ye, W. Hou, J. He and H. Zhao, *Appl Surf Sci*, 2023, **615**, 156413.

8 S. Dong, H. Zhou, X. Hu, J. Zhang, Y. Li, W. Shang, Z. Liu, L. Wan and H. Zhao, *Int J Hydrogen Energy*, 2023, **48**, 18233–18244.

9 J. Gild, Y. Zhang, T. Harrington, S. Jiang, T. Hu, M. C. Quinn, W. M. Mellor, N. Zhou, K. Vecchio and J. Luo, *Sci Rep*, 2016, **6**, 2–11.

10 J. Gild, A. Wright, K. Quiambao-Tomko, M. Qin, J. A. Tomko, M. Shafkat bin Hoque, J. L. Braun, B. Bloomfield, D. Martinez, T. Harrington, K. Vecchio, P. E. Hopkins and J. Luo, *Ceram Int*, 2020, **46**, 6906–6913.

11 C. Wang, M. Qin, T. Lei, Y. He, K. Kisslinger, T. J. Rupert, J. Luo and H. L. Xin, *J Eur Ceram Soc*, 2021, **41**, 5380–5387.

12 P. Sarker, T. Harrington, C. Toher, C. Oses, M. Samiee, J. P. Maria, D. W. Brenner, K. S. Vecchio and S. Curtarolo, *Nat Commun*, 2018, **9**, 1–10.

13 S. Guo, C. Ng, J. Lu and C. T. Liu, *J Appl Phys*, DOI:10.1063/1.3587228/984570.

14 R. Mitra, A. Bajpai and K. Biswas, *Ceram Int*, 2022, **48**, 16695–16706.

15 K. Yang, C. Oses and S. Curtarolo, *Chemistry of Materials*, 2016, **28**, 6484–6492.

16 S. Curtarolo, W. Setyawan, S. Wang, J. Xue, K. Yang, R. H. Taylor, L. J. Nelson, G. L. W. Hart, S. Sanvito, M. Buongiorno-Nardelli, N. Mingo and O. Levy, *Comput Mater Sci*, 2012, **58**, 227–235.

17 S. Curtarolo, W. Setyawan, G. L. W. Hart, M. Jahnatek, R. V. Chepulskii, R. H. Taylor, S. Wang, J. Xue, K. Yang, O. Levy, M. J. Mehl, H. T. Stokes, D. O. Demchenko and D. Morgan, *Comput Mater Sci*, 2012, **58**, 218–226.

18 C. E. Calderon, J. J. Plata, C. Toher, C. Oses, O. Levy, M. Fornari, A. Natan, M. J. Mehl, G. Hart, M. Buongiorno Nardelli and S. Curtarolo, *Comput Mater Sci*, 2015, **108**, 233–238.

19 F. Zhang. S.L. Chen, W. S. Cao, PandatTM software, CompuTherm LLC, Madison WI, USA, https://computherm.com/, (accessed 3 October 2023).

20 Y. Zhang, S. K. Sun, W. Zhang, Y. You, W. M. Guo, Z. W. Chen, J. H. Yuan and H. T. Lin, *Ceram Int*, 2020, **46**, 14299–14303.

21 M. Qin, S. Shivakumar, T. Lei, J. Gild, E. C. Hessong, H. Wang, K. S. Vecchio, T. J. Rupert and J. Luo, *J Eur Ceram Soc*, 2022, **42**, 5164–5171.

22 M. Li, X. Zhao, G. Shao, H. Wang, J. Zhu, W. Liu, B. Fan, H. Xu, H. Lu, Y. Zhou and R. Zhang, *Ceram Int*, 2021, **47**, 8707–8710.

23 L. Feng, F. Monteverde, W. G. Fahrenholtz and G. E. Hilmas, *Scr Mater*, 2021, **199**, 113855.

24 H. Meng, R. Yu, Z. Tang, Z. Wen, H. Yu and Y. Chu, *Acta Mater*, 2023, **256**, 119132.